Journal of Materials Chemistry C

RSC Publishing

PAPER

View Article Online
View Journal | View Issue

Cite this: *J. Mater. Chem. C*, 2013, **1**, 663

Influence of the chloro substituent on the mesomorphism of unsymmetrical achiral four-ring bent-core compounds: 2D polarization modulated banana phases†

Rahul Kanti Nath,[a] Rahul Deb,[a] Nirmalangshu Chakraborty,[a] Golam Mohiuddin,[a] Doddamane S. Shankar Rao[b] and Nandiraju V. S. Rao*[a]

Received 18th September 2012
Accepted 29th October 2012

DOI: 10.1039/c2tc00219a

www.rsc.org/MaterialsC

The synthesis and characterization of stable achiral unsymmetrical four-ring banana-shaped molecules consisting of a laterally chloro substituted 3,4′-disubstituted biphenyl unit with an ester linkage between the phenyl rings as the central unit in 4-(*N*-4′-*n*-tetradecyloxysalicylidene)aminophenyl [2-chloro-5-(*N*-4′-*n*-tetradecyloxysalicylidene) aminobenzoate] and 4-(*N*-4′-*n*-alkyloxysalicylidene) aminophenyl [4-chloro-5-(*N*-4′-*n*-alkyloxysalicylidene) aminobenzoate] are presented. These compounds are thermally and hydrolytically stable due to intramolecular hydrogen bonding and exhibit polarization splay modulated and layer undulated (PMLU) B7/$B1_{Rev/Tilted}$ (2D-polarization modulated layer undulated smectic phase, $B1_{RevTilt}$ phase) phase variants. The phase transitions have been confirmed by differential scanning calorimetry and the phases are characterized by polarized optical microscopy. Two representative examples have been characterized by X-ray diffraction studies. DFT calculations of the bending angle, dipole moments, molecular polarizabilities and voltage holding ratio are also presented.

1 Introduction

Discovery of mesogenic properties in banana or bent-shaped liquid crystals (LCs)[1,2] followed by their electrical and optical properties opened a new era in the field of shape dependent LCs.[3,4] Since then, many banana-shaped molecules have been synthesized and several reviews[5–10] have focused on the importance of these materials in applications. The majority of the bent-core mesogens reported in the literature contain five, six or seven phenyl rings. The variation in the number of aromatic units, the central bent core, lateral substituents and terminal groups in the molecule, with varying molecular interactions contribute to a significant modification in phase structure, as well as mesomorphism. The reduction of the number of phenyl rings to four can lower the transition temperatures, but the realization of mesophases in such four-ring compounds, in particular banana mesomorphism,[11–18] is elusive. However, recently a few reports have appeared in literature relating to four-ring systems exhibiting classical, as well banana mesomorphism.[19–22] Hird *et al.* reported[13] fluoro substituted bent-core compounds with chiral substituents exhibiting a monotropic nematic phase with chiral domains. They also reported[14,15] conventional calamitic phases. Matharu *et al.* reported[16] the synthesis of thiophene derivatives with a chiral centre in the end alkyl chain exhibiting chiral smectic phases. Aziz *et al.* reported[17] non-mesogenic dopants of banana-shaped meta substituted quaterphenyls consisting of three phenyl rings possessing an alkyl moiety at one end in a linear configuration with the fourth phenyl ring (possessing polar or alkyl substituents) substituted in the *meta*-position to enhance flexoelectric polarization. Weissflog *et al.* recently reported[18] asymmetric achiral four-ring bent-core mesogens derived from *N*-benzoylpiperazine and only a few of them were found to exhibit only calamitic phases. The introduction of a substituent in the side wings of the molecules also does not promote the mesomorphism. They reported polar structures under the influence of an electric field in these four-ring bent-core compounds exhibiting calamitic type smectic phases. Moreover they also exhibited a switchable smectic I phase, the first example of a non-chiral ferroelectric SmI phase ($SmIP_F$), which is attributed to the bent shape of the molecules. None of these four-ring compounds are found to spontaneously exhibit typical banana phases (SmAP, SmCP) because of weak steric interactions between the aromatic cores. Kang *et al.* reported[19] oxadiazole derivatives exhibiting a nematic-Bx phase variant. The typical banana (Bx) phase is uniaxial and found to exhibit a helical structure and chiral domains with weak birefringence. The chiral domains are randomly distributed domains of opposite handedness, and under the influence of an electric field

[a]*Chemistry Department, Assam University, Silchar-788011, India. E-mail: nandirajuv@gmail.com; Fax: +91 3842-270802; Tel: +91 3842270943*

[b]*Centre for Soft Matter Research, Jalahalli, Bangalore 560013, India. E-mail: shankar@csmr.res.in; Fax: +91 80 28382044; Tel: +91 80 28381119*

† Electronic supplementary information (ESI) available. See DOI: 10.1039/c2tc00219a

transformed to a homochiral SmC_AP_F phase with anti-ferroelectric response. However novel asymmetric fluorescent four-ring bent-core compounds[20,21] exhibiting banana mesomorphism *viz.*, 2D-polarization modulated layer undulated smectic phases (B7/$B1_{RevTilt}$ phases) have been reported. Fluoro substituted four-ring bent-core compounds[22] are found to exhibit columnar phases.

The four ring molecule possesses two OH groups in two wings, located in unsymmetrical positions, which deviates significantly from the typical symmetrical and/or V-shape of other bent core molecules. The modification of the angular 3,4′-disubstituted biphenyl unit with the introduction of an ester linkage, that is to say a COO moiety between the two phenyl units, leads to structural variation of the polar groups in bent core molecules and hence can promote a broad range of interesting variations in their mesogenic properties. Any substituent in the ortho position to an ester or imine linkage separating the two phenyl rings may substantially change the conformation of the molecule depending on the size, polarity and direction of the substituents. As a part of our work on four ring bent core systems we modified the central core with a substituent in the ortho position to the ester/imine moiety and introduced a bulky chloro substituent in the lateral position of the central bent core. Further the four ring molecule possesses an unequal distribution of aromatic rings in the two wings which manifests the unsymmetrical bent shaped molecule and hence can be regarded as true hockey stick molecules bordering the bent core and calamitic molecules.

Chloro substitution has been less studied,[23–25] compared to fluoro substitution. The chloro substituent (van der Waals radius = 1.75 Å) is larger than the fluoro (1.47 Å) or hydrogen (1.20 Å), and like hydrogen it is monoatomic. Because of the larger atomic size of the chloro substituent than the hydrogen and fluorine substituents it exerts a steric effect, as well as influencing the molecular interactions which is reflected in the organization of the molecular structures and in turn leads to interesting mesomorphic characteristics, that is to say a nematic phase with chiral domains and an optically isotropic banana phase. In this article we present the synthesis, mesomorphic behaviour, structural characterization and molecular characteristics using DFT study of a series of strongly nonsymmetrical hockey-stick-like mesogens with an ester linkage at the molecular bend and with a chloro substituent at two different positions of the central phenyl ring. The new compounds possess four aromatic rings, connected *via* ester and imine linkages. All the synthesized compounds (***n*R-4Cl, *n* = 10, 12, 14, 16; *n*R-2Cl, *n* = 14**; Scheme 1) exhibit typical banana phases which are described in section 3. Density functional theory (DFT) calculations[26] of minimized energies of the optimized conformation of the molecules, dipole moments, bend angles and molecular polarizabilities are presented in Section 3.3.

2 Experimental

All the chemicals were procured from M/s Alfa Aesar, Aldrich or Tokyo Kasei Kogyo Co. Ltd. The solvents and reagents were of AR grade and were distilled and dried before use. Micro analysis of C and H elements were determined on a Carlo-Erba 1106 elemental analyzer. IR spectra were recorded on a Perkin-Elmer L 120-000A spectrometer and Shimadzu IR Prestige-21, FTIR-8400S (ν_{max} in cm^{-1}) on KBr disks. The ^1H nuclear magnetic resonance spectra were recorded either on a JEOL FX-90Q (500 MHz) multinuclear spectrometer or Bruker DPX-400 spectrometer in $CDCl_3$ (chemical shift δ in parts per million) solution with TMS as the internal standard. UV visible absorption spectra of the compounds in $CHCl_3$ at different concentrations were recorded on a Shimadzu UV-1601PC spectrophotometer (λ_{max} in nm). Fluorescence spectra of the compounds in chloroform were recorded with a Shimadzu RF-5301PC Spectroflouorometer with a 150W xenon lamp as the excitation source. The liquid crystalline properties of the compounds were characterized using a polarizing microscope (Nikon optiphot-2-pol attached with hot and cold stage HCS302, with a STC200 temperature controller configured for HCS302 from INSTEC Inc. USA). The phase transition temperatures and associated enthalpies were recorded by differential scanning calorimetry (Perkin-Elmer Pyris-1 system) with a heating/cooling rate of 5°C min^{-1}. The details of the X-ray diffraction (XRD) studies carried out are given in ref. 27. The apparatus essentially involves a high-resolution X-ray powder diffractometer (PANalytical X'Pert PRO) equipped with a high-resolution fast detector PIXCEL.

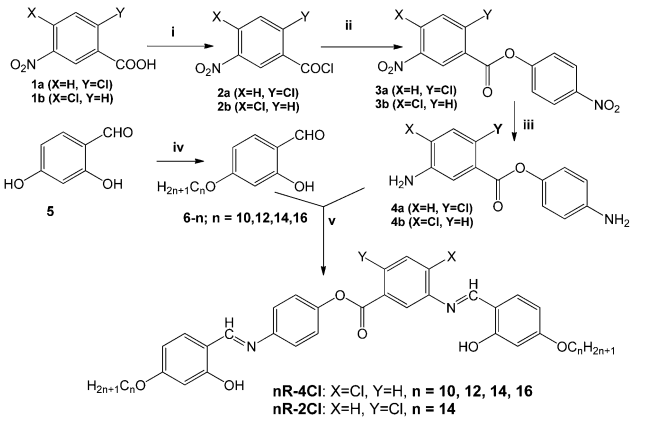

Scheme 1 (i) $SOCl_2$, DCM; (ii) 4 nitrophenol, DCM, K_2CO_3, TBAB, (iii) Pd/C (10%), H_2, ethylacetate (iv) acetone (dry), $NaHCO_3$, $C_nH_{2n+1}Br$, KI, Δ, 48 h, n = 10, 12, 14, 16 (v) AcOH, Δ, 3 h.

2.1 Synthesis

The synthesis of the chloro substituted compounds is described in Scheme 1. The central bent core moieties 4-aminophenyl 5-amino-2-chlorobenzoate (**4a**) and 4-aminophenyl 3-amino-4-chlorobenzoate (**4b**) were prepared as follows. 2-chloro 5-nitrobenzoic acid (**1a**) or 4-chloro-3-nitrobenzoic acid was converted into its acyl chloride (**2a** and **2b**) followed by condensation with 4-nitrophenol using a phase transfer reaction. The resultant 4-nitrophenyl 2-chloro-5-nitrobenzoate (**3a**) or 4-nitrophenyl 4-chloro-3-nitrobenzoate (**3b**) were subjected to a 10% Pd–C catalysed reduction to get the desired bent-core diamine (**4a** and **4b**). 4-*n*-alkyloxysalicylaldehyde was prepared by Williamson

etherification of 2,4-dihydroxybenzaldehyde (**5**) with the appropriate *n*-alkyl bromide. The condensation of 4-*n*-alkyloxy salicylaldehyde (**6**) with 4-aminophenyl 5-amino-2-chlorobenzoate in the presence of a few drops of glacial acetic acid yielded the target bent shaped compounds 4-(*N*-4′-*n*-alkyloxysalicylidene)aminophenyl [4-chloro-3-(*N*-4′-*n*-alkyloxysalicylidene)aminobenzoate] (***n*R-4Cl, *n* = 10, 12, 14, 16**) and 4-(*N*-4′-*n*-alkyloxysalicylidene)aminophenyl [2-chloro-5-(*N*-4′-*n*-alkyloxysalicylidene)aminobenzoate] (***n*R-2Cl, *n* = 14**). To avoid the formation of side products, the precipitated compounds were filtered when the solution was hot to yield the pure compounds. The compounds were further recrystallized repeatedly to get the pure samples. The formation of all of the compounds was confirmed by ^{1}H NMR and IR spectroscopy and the composition of the compounds purity was established by elemental analysis. The details of the experimental procedures along with the spectroscopic data for all the compounds are presented in the ESI.† The liquid-crystalline behaviour of the synthesised compounds were investigated by polarizing optical microscopy (POM), differential scanning calorimetry (DSC) and X-ray studies.

3 Results and discussion

3.1 Mesomorphic properties

The transition temperatures, enthalpies and entropies associated with the phase transitions of the compounds **14R-2Cl** and of the homologous series ***n*R-4Cl** (***n* = 10, 12, 14, 16**) which were obtained from DSC at a scan rate of 5 °C min^{-1} in the second heating and cooling scans are presented in Table 1. All the compounds of the homologous series (***n*R-4Cl**) show enantiotropic mesomorphic behaviour for a moderate temperature range. The lower homologues of the series (**10R-4Cl** and **12R-4Cl**) show characteristic textures of the B1 mesophase whereas higher homologues (**14R-4Cl** and **16R-4Cl**) exhibit optical textures resembling the B7 phase.

14R-2Cl. On slow cooling from the isotropic phase of the compound, the growth of the mesophase is reflected in the form of telephone-wire structures resembling the B7 phase which are shown in Fig. 1a followed by dendritic growth (Fig. 1b). Further cooling of the sample revealed a fully grown structured columnar fan like texture under the polarization microscope. It exhibits pseudo-broken fans or circular domains with extinction brushes directed along polarizer directions (Fig. 1c). With decreasing temperature low birefringent stripes appeared across the blades of the columnar fan (Fig. 1d and e) and finally became uniform (Fig. 1f) without any changes in the columnar texture before it crystallizes. The transient transition bars of arcs across the fans at 125.0 °C as a function of time gave an impression of a phase transition, but no such phenomenon was confirmed by other methods.

16R-4Cl and 10R-Cl. Upon very slow cooling the isotropic liquid, the mesophase defect textures exhibited by **16R-4Cl** (Fig. 2a–g) resembled the B7 phase[28–31] texture of fascinating long spiral domains. If the isotropic liquid is cooled down very fast, the B7 phase appears as a cluster of thin thread-like or straight lancet-like nuclei (Fig. 2g) which coalesce to an

Table 1 Transition temperatures (°C), enthalpies (kJ mol^{-1}) and entropies (J mol^{-1} K^{-1}) of **14R-2Cl** and other homologues of ***n*R-4Cl (*n* = 10, 12, 14, 16)** (the first row indicates the second heating cycle and the second row indicates the second cooling cycle)

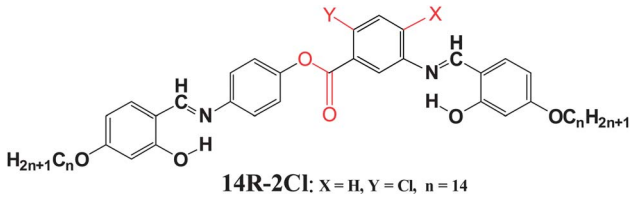

14R-2Cl: X = H, Y = Cl, n = 14
nR-4Cl: X = Cl, Y = H, n = 10, 12, 14, 16

Compound	Cr	Heating Cooling	B1/B7[a]	Heating Cooling	I
14R-2Cl	•	130.7 [*35.9*, *88.2*]	•	134.7 [*7.1*, *17.4*]	•
	•	109.6 [*40.7*, *106.3*]	•	133.6 [12.7, *42.3*]	•
10R-4Cl	•	126.9 [*21.4*, *53.6*]	•	127.5[a]	•
	•	83.4[24.3, 68.1]	•	127.2 [*8.1*, *20.2*]	•
12R-4Cl	•	133.2 [*37.1*, *91.4*]	•	134.8 [*0.2*, *0.5*]	•
	•	110.6 [*34.7*, *90.3*]	•	132.9 [*6.3*, *15.6*]	•
14R-4Cl	•	131.3 [*47.8*, *118.2*]	•	137.4 [*17.0*, *41.5*]	•
	•	111.8 [*42.8*, *111.3*]	•	136.7 [*16.5*, *40.3*]	•
16R-4Cl	•	130.0 [*41.2*, *102.2*]	•	132.4 [*1.4*, *3.5*]	•
	•	108.7 [*54.2*, *141.9*]	•	131.3 [6.9, *17.2*]	•

[a] The compounds **10R-4Cl** and **12R-4Cl** exhibit the $B1_{Revtilted}$ mesophase whereas **14R-4Cl, 16R-4Cl** and **14R-2Cl** exhibit the B7 mesophase.

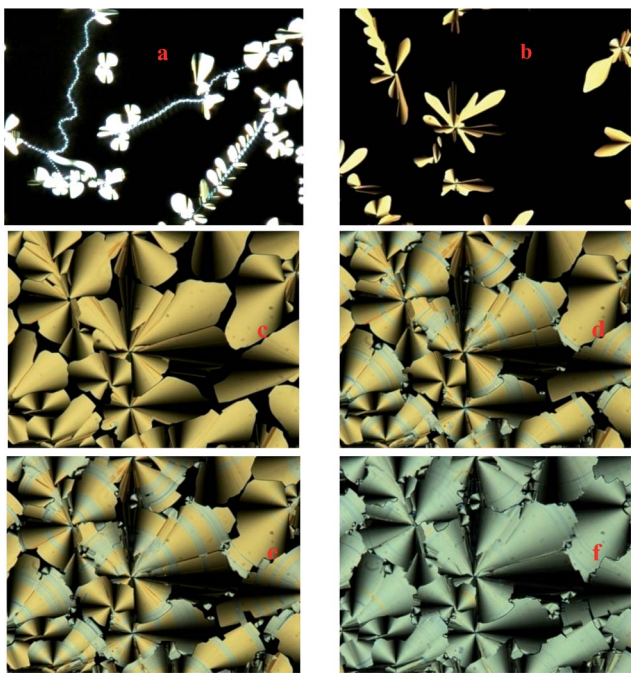

Fig. 1 Photomicrographs of the compound **14R-2Cl** in a 3.5 μm homogenous cell. (a) Helical spiral formation from the isotropic phase to the mesomorphic phase at 133.6 °C, (b) dendritic growth at 133.6 °C, (c) fully developed columnar texture, (d) and (e) at 125.0 °C after 5 and 10 minutes and (f) with a change in colour at 124 °C.

unspecific texture. On slow cooling (0.01 °C min^{-1}), varieties of textures are obtained, but these mostly occur simultaneously within the same preparation. Also, on slow cooling of the isotropic liquid, the B7 phase frequently forms elongated germs such as straight lancet-like or irregular thread-like germs. But frequently these germs clearly have a spiral or double-spiral character. Fig. 2g shows the growth of a spiral germ. The handedness of the screw-like nuclei could be determined by adjusting the focus of the microscope. The B7 phase frequently grows as oval or sometimes as circular domains. Such domains (shown in Fig. 2a, b and f) exhibit equidistant stripes. The compound **10R-4Cl** exhibited a columnar fan like or a telephone like texture connecting the focal conic domains (Fig. 3a–d). Hence the lower homologues are exhibiting a $B1_{Revtilted}$ phase while the higher homologues are exhibiting B7 like phases.

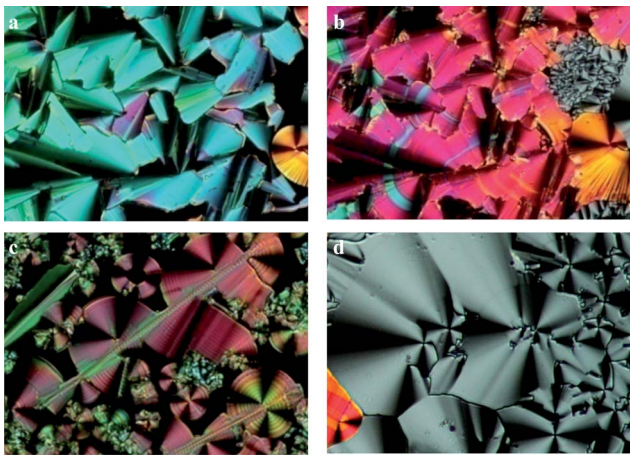

Fig. 3 Polarising optical photographs of **14R-4Cl** on a HTAB treated cell at (a) 133.2 °C, (b) 124.8 °C, (c) nylon 6,6 treated cell at 131 °C, and (d) Different location of HTAB treated cell at 124.8 °C.

3.2 X-ray studies

14R-2Cl. To get information on the structural aspects, XRD measurements were carried out on the B7 mesophase for the compound **14R-2Cl**. Representative diffractograms (intensity *versus* 2θ profile) in the mesophase at 130 °C are shown in Fig. 4. The broad diffuse peak in the high angle region (inset (b)), corresponding to a spacing of 4.61 Å, together with the sharp intense reflections in the low angle region, establishes the layering order of the mesophase. There are four sharp peaks in the low angle region. The spacing obtained from the profile fitting procedure is tabulated in Table 2. The low angle intense sharp peak with spacing 47.32 Å corresponds to layer periodicity. This spacing is lower than the calculated molecular length of 56.7 Å in the most extended conformation in the gaseous phase (see Fig. 4d) although it is likely that the somewhat more bent conformation is adopted in the condensed phases. The difference in the spacings (measured layer spacing and calculated molecular length) suggests that the molecules are tilted in the layer with the amount of tilt angle being 33 deg in the mesophase. All low angle peaks can be indexed to a rectangular lattice which indicates that the molecules are arranged in a two-dimensional (2D) lattice within the layer. Inset (c) shows thermal variation of the layer spacing (d) for the compound **14R-2Cl**. The spacing d increases with decreasing temperature in the B7 phase with extracted slope dd/dT values being $= -4.8 \times 10^{-2}$ Å K^{-1}. The negative thermal expansion is due to the stretching of the alkyl chains with a decrease in temperature. Another reflection in the low angle region (not marked in the figure at $2\theta \sim 1.26°$) indicative of in-plane modulation of the smectic layers of wavelength $\lambda \sim 70.1$ Å associated with the 2D polarization splay modulated layer undulated structure, a structural feature associated with the $B_7/B1_{RevTilted}$ phases with a 2D lattice. The quantum mechanical calculations (to be described later) were performed with density functional theory (DFT),[26] by employing the combination of B3LYP functional and 6–31 g(d,p) basis set using the Gaussian 09 package.

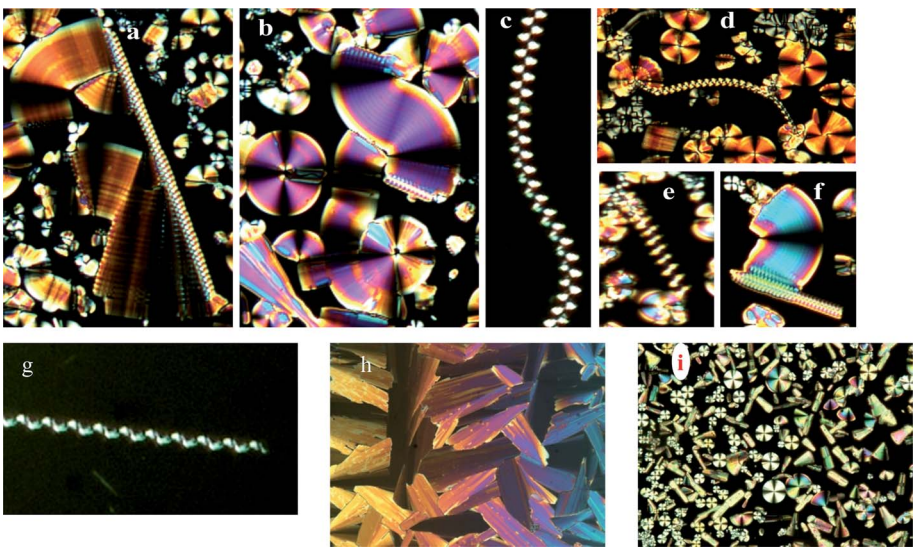

Fig. 2 Polarising optical microphotographs of various features of B7 textures of compounds **16R-4Cl** sandwiched between a glass plate and cover slip (a–g). (h) **16R-4Cl** in a 5 μm cell at 132 °C. (i) Texture of **10R-4Cl** at 134.2 °C.

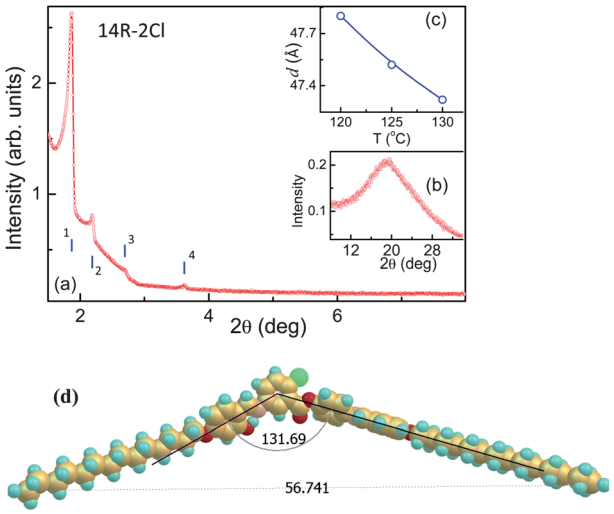

Fig. 4 (a) Intensity *versus* 2θ profile in the low angle region for the compound **14R-2Cl** at $T = 130$ °C in the B7 mesophase. Inset (b) shows the diffuse peak in the high angle region reflecting the liquid-like ordering of the layers. Inset (c) shows the thermal variation of layer spacing d in the mesophase. The solid line serves as a guide for the eye. (d) A space filling model of the energy minimised molecular structure of the molecule **14R-2Cl** with a fully extended chain in trans conformation (56.7 Å).

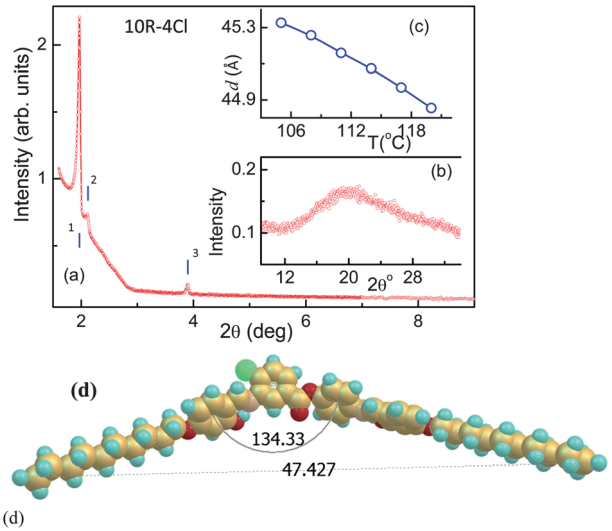

Fig. 5 (a) Intensity *versus* 2θ profile in the low angle region for the compound **10R-4Cl** at $T = 120$ °C. Inset (b) shows a diffuse peak in the high angle region reflecting the liquid-like ordering of the layers. Inset (c) shows thermal variation of layer spacing d in the mesophase. The solid line serves as a guide for the eye. (d) Fully extended all trans conformation of **10R-4Cl**.

Table 2 XRD data of the two compounds studied. For both the compounds the columnar axis is taken as the *c*-axis and *ab* the lattice plane (hk values index the reflecting planes)

	d_{meas} (Å)	d_{calc} (Å)	(hk)
14R-2Cl $T = 130$ °C			
1	47.32	47.32	(10)
2	40.39	40.39	(01)
3	32.80	30.72	(11)
4	24.41	23.66	(20)
5	4.61		
$a = 47.32$ Å; $b = 40.39$ Å; $c = 4.61$ Å; $V = 8816.4$ Å^3			
10R-4Cl $T = 120$ °C			
1	44.86	44.86	(10)
2	41.67	41.67	(01)
3	22.67	22.43	(20)
4	4.41		
$a = 44.86$ Å; $b = 41.67$ Å; $c = 4.41$ Å; $V = 8238.7$ Å^3			

10R-4Cl. XRD measurements were also carried out on another compound **10R-4Cl** which shows B1 mesophase. Fig. 5 shows the intensity *versus* 2θ profile taken at 120 °C. It shows three sharp peaks in the low angle region (inset (a)) with a broad diffuse peak in the high angle region (inset (b)) corresponding to a spacing of 4.41 Å. The broad diffuse peak in the wide angle region reflected the lateral spacing between the molecules and corresponded to the short-range order of molten aliphatic chains indicative of a liquid like in-plane order of the fluid phase (Fig. 5b). The sharp intense peak in the low angle region along with the diffuse wide angle peak establishes the layering order of the B1 phase. The spacings of the three sharp peaks in the low angle regions are tabulated in Table 2. The intense low angle peak with a spacing of 44.86 Å corresponds to the layer periodicity (d). This spacing is lower compared to the calculated molecular length of 47.43 in the all trans conformation (see Fig. 5d). This suggests that the molecules were tilted within a layer with the tilt angle being 19°. All the low angle peaks are indexed to a primitive rectangular lattice (see Table 2). The XRD measurements confirm that the molecules are packed in a columnar arrangement with a 2D rectangular lattice within the layer. Inset (c) of Fig. 5 shows the thermal variation of layer spacing for the compound **10R-4Cl** in the B1 mesophase. The spacing d increases with decreasing temperature with the slope equal to $dd/dT = -3.14 \times 10^{-2}$ Å K^{-1}. As explained earlier the negative thermal expansion is due to the stretching of alkyl chains with a decrease in temperature.

The formation of stripes on focal conic textures, the multiple peak reflections at low angles and the tilt in molecular layering and non-switchable phase structure are indicative of a $B1_{RevTilted}$ phase structure and suggest that the phase represents the 2D polarization splay modulated layer undulated molecular structure of the SmCPU family.[32–34]

3.3 DFT calculations

DFT computational studies based on quantum mechanical calculations were performed to obtain the information related to molecular conformation, bend angle, dipole moment, molecular polarizability and electrostatic potential distribution of the selected molecules **14R-2Cl** and **14R-4Cl**. Full geometry optimizations have been carried out without imposing any constraints using the Gaussian 09 program package.[25] Spin-restricted DFT calculations were carried out in the framework of the generalized gradient approximation (GGA) using Becke3–Lee–Yang–Parr hybrid functional (B3LYP) exchange-correlation

functional and the 6-31G (d, p) basis set.[35,36] B3LYP functional with the standard basis set 6-31G have been used due to its successful application for larger organic molecules, as well as hydrogen bonded systems in the past,[37–39] and bent core molecules[40–43] recently.

The difference in bond lengths (56.74 Å and 56.96 Å) and bend angles (131° and 134°) among the two studied compounds **14R-2Cl** and **14R-4Cl** (Table 3) is not significant. But the variation in dipole moment is significant. The dipole moment of **14R-2Cl** is 5.07 D whereas **14R-4Cl** it is 3.65 D. The major contribution of the dipole moment comes from the X and Z components of **14R-2Cl** whereas in the case of **14R-4Cl** the major role in the dipole moment is played by the Z component. Polarizabilities are crucial for an understanding of the molecular properties in molecular optics and spectroscopy. Electrostatic intermolecular interaction energy is related to this quantity, in particular for systems without a permanent dipole moment.[44]

DFT calculated principal polarizability components (α_{XX}, α_{YY}, α_{ZZ}), isotropic polarizability component α^{iso}, polarizability anisotropy $\Delta\alpha = [\alpha_{XX} - (\alpha_{YY} + \alpha_{ZZ})/2]$ and asymmetry parameter, $\eta = [(\alpha_{YY} - \alpha_{ZZ})/(\alpha_{XX} - \alpha^{iso})]$, parameters relative to the molecular polarizability tensor, α, in the Cartesian reference frame are displayed in Table 4. The molecular polarizability component α_{XX} is comparatively larger along the molecular longitudinal *X*-axis (Fig. 6) for both the molecules (**14R-2Cl** and **14R-4Cl**) than the other two directions. The asymmetry parameter $\eta = [(\alpha_{YY} - \alpha_{ZZ})/(\alpha_{XX} - \alpha^{iso})]$, which is dependent on the bending angle ~138°, is found to be same for both the molecules (0.349 and 0.352 respectively for the molecules **14R-2Cl** and **14R-4Cl**). The principle components of the polarizability tensor (α_{XX}, α_{YY}, α_{ZZ}) and $\alpha^{iso} = (\alpha_{XX} + \alpha_{YY} + \alpha_{ZZ})/3$ is rather small. Although the molecular formula and number of electrons of the two studied molecules are the same, the main component of static polarizability along the molecular long *X*-axis differs significantly due to the different position of the chlorine atom in the central ring and also magnitude of the dipole moment.

In active matrix displays (AMD) the high voltage holding capability of the liquid crystalline materials in matrix elements is required for better contrast and flickering. In TFT-LCD applications, the voltage holding ratio (VHR) is defined as the ratio of the voltages at a pixel at the end and the beginning of the frame time[45,46] which is a crucial requirement in order to avoid image sticking.[47] The VHR values can be correlated with electrostatic potentials (ESP) and an even charge distribution correlates reasonably well with the high voltage holding ratio of the material. Fig. 7a and b display the isoelectron density surface of **14R-2Cl** and **14R-4Cl** respectively. In both the molecules, the positive electrostatic potential is homogenously distributed except the three negative ESP centers[48] (light red colour contours) favoring weak interactions with cations. The absence of a red coloration in the ESP contour in the majority surface area of the molecule denotes a relatively high VHR value. Hence homogenous distribution of partial charges lowers the ability to form cationic complexes by local electrostatic interactions and correlates reasonably well with the high VHR of the material. From the total ESP surface it is clear that the electron density is almost homogeneously distributed in molecules which indicate the applicability of this type of molecule in mixtures and also gives an indication to the design of the molecules.

Table 4 DFT calculated principal polarizability components (α_{XX}, α_{YY}, α_{ZZ}), isotropic component $\alpha^{iso} = (\alpha_{XX} + \alpha_{YY} + \alpha_{ZZ})/3$, anisotropy $\Delta\alpha = [\alpha_{XX} - (\alpha_{YY} + \alpha_{ZZ})/2]$ and asymmetry, $\eta = [(\alpha_{YY} - \alpha_{ZZ})/(\alpha_{XX} - \alpha^{iso})]$[a]

Compound	α_{XX}	α_{YY}	α_{ZZ}	α_{iso}	$\Delta\alpha$	η_α
14R-2Cl	1275	609	433	772	754	0.349
14R-4Cl	1220	604	440	755	698	0.352

[a] All polarizability components and the anisotropy parameter are expressed in Bohr^3 (with 1 Bohr = 0.52917 Å).

3.4 UV-visible and fluorescence studies

The emission properties of organic LCs are currently an active area of research due to their potential applications in opto-electronics. Emissive liquid crystals are intriguing systems for materials research because they couple molecular self-assembly with intrinsic light generation capability. The substituent on the central core plays an important role in the modification of the electronic characteristics of the molecules. Hence the absorption and emission properties of the compounds were studied and the results are presented below.

The UV-visible absorption and fluorescence spectroscopic properties of the two representative compounds **14R-2Cl** and **14R-4Cl** in chloroform (conc. 1.0×10^{-5} M) were studied in solution at different concentrations in a range of solvents, to obtain information regarding absorption and emission maxima and the Stokes shift of fluorescence. The UV-visible spectra in these homologous compounds exhibited strong absorption peaks at ~346 nm with a large molar extinction coefficient (Fig. 8, 3.58 eV for **14R-2Cl**, $\varepsilon \sim 216\,000$ L mol^{-1} cm^{-1} and 3.58 eV for **14R-4Cl**, $\varepsilon \sim 140\,000$ L mol^{-1} cm^{-1}

Table 3 DFT calculated minimized energy, dipole moment components (μ_X, μ_Y, μ_Z), modulus (μ), bend angle (θ) and molecular length of the two molecules

		Dipole moment (Debye)					
Compound	Energy (a.u.)	μ_x	μ_y	μ_z	$\mu_{resultant} = (\mu_x^2 + \mu_y^2 + \mu_z^2)^{1/2}$	Bend angle (degree)	Molecular length (Å)
14R-2Cl	−3162.252	3.26	2.69	6.26	7.55	131.7	56.74
14R-4Cl	−3162.258	0.56	2.06	6.22	6.58	134.5	56.96

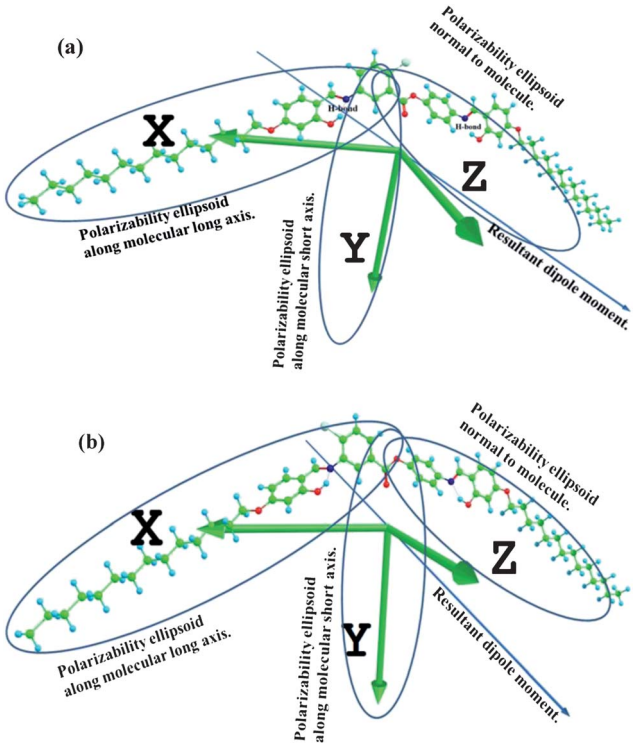

Fig. 6 Molecular polarizability ellipsoid and direction of the resultant dipole moment of (a) **14R-2Cl** and (b) **14R-4Cl**.

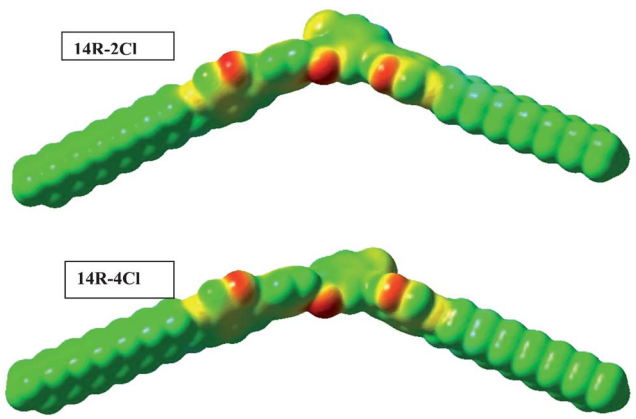

Fig. 7 Isoelectron density surface with electrostatic potential of (a) **14R-2Cl** (b) **14R-4Cl** Red and sky-blue surfaces indicate negative and positive electrostatic potential respectively.

concentration = 10^{-5} M solution in $CHCl_3$). The strong absorption band reflects the π–π* transition of the highly π-conjugated system having the substituted phenyl benzoate unit as the core. Both the compounds were found to exhibit a large Stokes shift (~100 nm), which reflects the structural relaxation of the excited molecule, and is significantly larger than that reported in push–pull systems exhibiting liquid crystal behaviour,[49–53] reflecting changes in the molecular conformation upon excitation. These results are in good agreement with the reported results of molecular J-aggregates[54] in which the

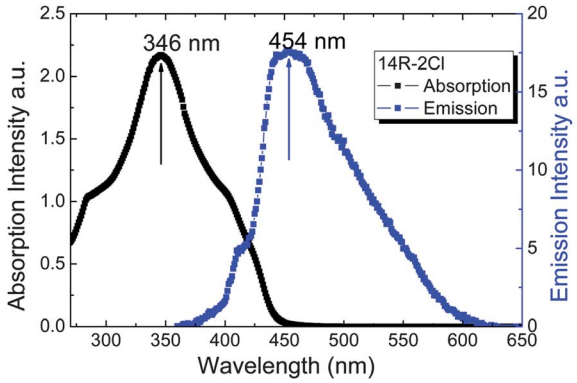

Fig. 8 UV-visible and fluorescent spectra of **14R-2Cl** and **14R-4Cl** in chloroform ($C = 10^{-5}$).

excitonic energy is delocalized as a result of intermolecular coupling within the head-to-tail arrangement of the molecules in the solution.

4 Conclusions

Summarizing the results, the four ring compounds under discussion resemble typical hockey-stick shapes and were found to exhibit typical banana phases, that is to say layer undulated non-switchable $B7/B1_{Rev\ Tilted}$ phases. These bent shapes possessed a bend angle of 130–135° from DFT study and still exhibit banana mesomorphism. The present work demonstrated that banana mesomorphism can be realized in four-ring banana shaped compounds which are at the interface between the calamitic and banana-shaped liquid crystals. Hence the induction of such mesomorphic characteristics are dependent on several factors, including linking groups, the length of the end alkyl chains, the nature and position of substituents, steric interactions *etc.* DFT study indicated the presence of homogeneously distributed electron density and the negligible negative electrostatic potential in these molecules.

Acknowledgements

Financial assistance provided by the Department of Science and Technology, University Grants Commission and Department of Atomic Energy, India are gratefully acknowledged.

References

1 M. Kuboshita, Y. Matsunaga and H. Matsuzaki, *Mol. Cryst. Liq. Cryst.*, 1991, **199**, 319.
2 T. Matsuda and Y. Matsunaga, *Bull. Chem. Soc. Jpn.*, 1991, **64**, 2192.
3 T. Niori, J. Sekine, J. Watanabe, T. Furukava and H. Takezoe, *J. Mater. Chem.*, 1996, **6**, 1231.
4 D. R. Link, G. Natale, R. Shao, J. E. Maclennan, N. A. Clark, E. Korblova and D. M. Walba, *Science*, 1997, **278**, 1924.
5 G. Pelzl, S. Diele and W. Weissflog, *Adv. Mater.*, 1999, **11**, 707.
6 R. A. Reddy and C. Tschierske, *J. Mater. Chem.*, 2006, **16**, 907.

7 H. Takezoe and Y. Takanishi, *Jpn. J. Appl. Phys.*, 2006, **45**, 597.
8 C. Tschierske and G. Dantlgraber, *Pramana*, 2003, **61**, 455.
9 M. B. Ros, J. L. Serrano, M. R. de la Fuente and C. L. Folcia, *J. Mater. Chem.*, 2005, **15**, 5093.
10 A. Jakli, C. Bailey and J. Harden, *Thermotropic Liquid Crystals*, ed. A. Ramamoorthy, Springer, The Netherlands, 2007, pp. 59–83.
11 F. C. Yu and L. J. Yu, *Chem. Mater.*, 2006, **18**, 5410.
12 J. H. Wild, K. Bartle, M. O'Neill, S. M. Kelly and R. P. Tuffin, *Liq. Cryst.*, 2006, **33**, 635.
13 M. Hird, Y. Raoul, J. W. Goodby and J. Gleeson, *Ferroelectrics*, 2004, **309**, 95.
14 K. M. Fergusson and M. Hird, *J. Mater. Chem.*, 2010, **20**, 3069; K. M. Fergusson and M. Hird, *Adv. Mater.*, 2007, **19**, 211.
15 M. Hird, J. W. Goodby, J. Gough and K. J. Toyne, *J. Mater. Chem.*, 2001, **11**, 2732.
16 A. S. Matharu, C. Grover, L. Komitov and G. Anderson, *J. Mater. Chem.*, 2000, **10**, 1303.
17 N. Aziz, S. M. Kelly, W. Duffy and M. Goulding, *Liq. Cryst.*, 2008, **35**, 1279.
18 W. Weissflog, U. Dunemann, S. F. Tandel, M. G. Tamba, H. Kresse, G. Pelzl, S. Diele, U. Baumeister, A. Eremin, S. Stern and R. Stannarius, *Soft Matter*, 2009, **5**, 1840.
19 S. Kang, Y. Saito, N. Watanabe, M. Tokita, Y. Takanishi, H. Takezoe and J. Watanabe, *J. Phys. Chem. B*, 2006, **110**, 5205.
20 R. Deb, R. K. Nath, M. K. Paul, N. V. S. Rao, F. Tuluri, Y. Shen, R. Shao, D. Chen, C. Zhu, I. I. Smalyukh and N. A. Clark, *J. Mater. Chem.*, 2010, **20**, 7332.
21 D. K. Yoon, R. Deb, D. Chen, E. Korblova, R. Shao, K. Ishikawa, N. V. S. Rao, D. M. Walba, I. I. Smalyukh and N. A. Clark, *Proc. Natl. Acad. Sci. U. S. A.*, 2010, **107**, 21311.
22 R. K. Nath, D. D. Sarkar, D. S. S. Rao and N. V. S. Rao, *Liq. Cryst.*, 2012, **39**, 889.
23 W. Weissflog, U. Dunemann, M. W. Schroder, S. Diele, G. Pelzl, H. Kresse and S. Grande, *J. Mater. Chem.*, 2005, **15**, 939.
24 W. Weissflog, S. Sokolowski, H. Dehne, B. Das, S. Grande, M. W. Schroder, A. Eremin, S. Diele, G. Pelzl and H. Kresse, *Liq. Cryst.*, 2004, **31**, 923.
25 S. Kang, J. Thisayukta, H. Takezoe, J. Watanabe, T. Ogino, T. Doi and T. Takahashi, *Liq. Cryst.*, 2004, **31**, 1323.
26 M. J. Frisch*et al.*, *GAUSSIAN 09 (Revision B.01)*, Gaussian, Inc., Wallingford, CT, 2010.
27 S. K. Prasad, D. S. S. Rao, S. Sridevi, C. V. Lobo, B. R. Ratna, J. Naciri and R. Shashidhar, *Phys. Rev. Lett.*, 2009, **102**, 1478021.
28 G. Pelzl, S. Diele, A. Jakli and W. Weissflog, *Liq. Cryst.*, 2006, **33**, 1513.
29 J. Szydlowska, J. Mieczkowski, J. Matraszek, D. W. Bruce, E. Gorecka, D. Pociecha and D. Guillon, *Phys. Rev. E: Stat. Phys., Plasmas, Fluids, Relat. Interdiscip. Top.*, 2003, **67**, 031702.
30 J. Svoboda, V. Novotna, V. Kozmik, M. Glogarova, W. Weissflog, S. Diele and G. Pelzl, *J. Mater. Chem.*, 2003, **13**, 2104.
31 M. Kohout, J. Svoboda, V. Novotna, D. Pociecha, M. Glogarova and E. Gorecka, *J. Mater. Chem.*, 2009, **19**, 3153.
32 D. A. Coleman, C. D. Jones, M. Nakata, N. A. Clark, D. M. Walba, W. Weissflog, K. Fodor-Csorba, J. Watanabe, V. Novotna and V. Hamplova, *Phys. Rev. E: Stat., Nonlinear, Soft Matter Phys.*, 2008, **77**, 021703.
33 C. L. Folcia, J. Etxebarria, J. Ortega and M. B. Ros, *Phys. Rev. E: Stat., Nonlinear, Soft Matter Phys.*, 2005, **72**, 041709.
34 D. Pociecha, N. Vaupotic, E. Gorecka, J. Mieczkowski and K. Gomola, *J. Mater. Chem.*, 2008, **18**, 881.
35 K. Kim and K. D. Jordan, *J. Phys. Chem.*, 1994, **98**, 10089.
36 P. J. Stephens, F. J. Devlin, C. F. Chabalowski and M. J. Frisch, *J. Phys. Chem.*, 1994, **98**, 11623.
37 A. R. Leach, *Molecular Modelling – Principles and Applications*, Pearson education limited, England, 2nd edn, 2001.
38 N. H. March, *Electron Density Theory of Atoms and Molecules*, Academic, London, 1992.
39 E. S. Kryachko and E. V. Ludena, *Energy Density Functional Theory of Many-Electron System*, Kluwer, Dordrecht, 1990.
40 J. Seltmann, A. Marini, B. Mennucci, S. Dey, S. Kumar and M. Lehmann, *Chem. Mater.*, 2011, **23**, 2630.
41 A. R. K. Selvaraj, W. Weissflog and R. Friedemann, *J. Mol. Model.*, 2007, **13**, 907.
42 A. R. K. Selvaraj, W. Weissflog, G. Pelzl, S. Diele, H. Kresse, Z. Vakhovskaya and R. J. Friedemann, *Phys. Chem. Chem. Phys.*, 2006, **8**, 1170.
43 W. Weissflog, G. Naumann, B. Kosata, M. W. Schroeder, A. Eremin, S. Diele, H. Kresse, R. Friedemann, A. R. K. Selvaraj and G. Pelzl, *J. Mater. Chem.*, 2005, **15**, 4328.
44 W. Koch and M. C. Holthausen, *A Chemist's Guide to Density Functional Theory*, Wiley-VCH Verlag GmbH, 2nd edn, 2001.
45 A. Sasaki, T. Uchida and S. Miyagami, *Japan Display*, 1986, p. 62.
46 M. Schadt, *Displays*, 1992, **13**, 11.
47 J. Jin Yan, H. C. Cheng, L. Rao, T. Ishinabe and S. T. Wu, *Proc. of China Display/Asia Display*, 2011, 69.
48 S. Mecozzi, Jr, A. P. West and D. A. Dougherty, *Proc. Natl. Acad. Sci. U. S. A.*, 1996, **93**, 10566.
49 H. Gallardo, R. Cristiano, A. Vieira, R. A. W. Neves Filho, R. M. Srivastava and I. H. Bechtold, *Liq. Cryst.*, 2008, **35**, 57.
50 A. Vieira, R. Cristiano, A. J. Bortoluzzi and H. Gallardo, *J. Mol. Struct.*, 2008, **875**, 364.
51 R. M. Srivastava, R. A. W. Neves Filho, R. Schneider, A. Vieira and H. Gallardo, *Liq. Cryst.*, 2008, **35**, 737.
52 R. Cristiano, F. Ely and H. Gallardo, *Liq. Cryst.*, 2005, **32**, 15.
53 A. Vieira, R. Cristiano, F. Ely and H. Gallardo, *Liq. Cryst.*, 2006, **33**, 381.
54 F. Camerel, L. Bonardi, M. Schmutz and R. Ziessel, *J. Am. Chem. Soc.*, 2006, **128**, 4548.

